ADVANCES IN ATMOSPHERIC SCIENCES, VOL. 22, NO. 1, 2005, 90–102

An Improved Method for Doppler Wind and Thermodynamic Retrievals

SHUN Liu[1,3] (刘 舜), QIU Chongjian[*1] (邱崇践), XU Qin[2] (许 秦), ZHANG Pengfei[3] (张芃菲), GAO Jidong[4] (郜吉东)，and SHAO Aimei[1] (邵爱梅)

[1] *College of Atmosphereic Sciences, Lanzhou University, Lanzhou, Gansu* 730000

[2] *National Severe Storms Laboratory, Norman, Oklahoma, USA* 73069

[3] *Cooperative Institute for Mesoscale Meteorological Studies, Norman, Oklahoma, USA* 73069

[4] *Center for Analysis and Prediction of Storms, Norman, Oklahoma, USA* 73069

(Received 24 February 2004; revised 16 July 2004)

ABSTRACT

A variational method is developed to retrieve winds in the first step and then thermodynamic fields in the second step from Doppler radar observations. In the first step, wind fields are retrieved at two time levels: the beginning and ending times of the data assimilation period, simultaneously from two successive volume scans by using the weak form constraints provided by the mass continuity and vorticity equations. As the retrieved wind fields are expressed by Legendre polynomial expansions at the beginning and ending times, the time tendency term in the vorticity equation can be conveniently formulated, and the retrieved winds can be compared with the radar observed radial winds in the cost function at the precise time and position of each radar beam. In the second step, the perturbation pressure and temperature fields at the middle time are then derived from the retrieved wind fields and the velocity time tendency by using the weak form constraints provided by the three momentum equations. The merits of the new method are demonstrated by numerical experiments with simulated radar observations and compared with the traditional least squares methods which consider neither the precise observation times and positions nor the velocity time tendency. The new method is also applied to real radar data for a heavy rainfall event during the 2001 Meiyu season in China.

Key words:

1. Introduction

Modern Doppler radars have the ability to scan large volumes of the atmosphere at high space and time resolutions. High-resolution radar measurements have provided unprecedented opportunities for high-resolution weather analyses, and many different types of methods have been developed in recent years to analyze and retrieve high-resolution wind and thermodynamic fields from Doppler radar wind. Among the existing methods, the least squares methods are relatively simple and often very efficient in comparison with the adjoint method (Sun and Crook, 1994, 1996; Xu et al., 1994, 2001). Various least squares methods have been widely used for three-dimensional wind and thermodynamic analyses by using the weak form constraints provided by the continuity, momentum and/or vorticity equations (Scialom and Lemaître, 1990; Laroche and Zawadzki, 1994; Shapiro et al., 1995; Qiu and Xu, 1996; Zhang and Gal-Chen, 1996; Gao et al., 1999; Liou 1999; Weygandt et al., 2002).

In the traditional least squares methods, retrievals are performed at a single time level. Measurements at different beam locations (thus at different times) in a volume scan were traditionally assumed to be instantaneous for the entire volume scan (Qiu and Xu, 1996; Liou, 1999) or interpolated to the analysis time in the observation space (Clark et al., 1980; Protat and Zawadzki, 1999, 2000). However, interpolations in the observation space often require collocated or approximately collocated measurements from the two volume scans. Obviously, no time interpolation can

*E-mail: qiucj@lzu.edu.cn

be performed in regions where data "holes" exist in either volume scan. Thus, time interpolations in the measurement space are often difficult or impractical. Because of this, radar data from one volume scan are treated as observations at a single time level in the traditional least square methods, although it is well known that this treatment is a potentially significant source of error for a fast-evolution weather system. As the time tendency of the retrieved wind is not available in the traditional least squares methods, the time tendency terms in the momentum equations (Liou, 2001; Liou et al., 2003) or in the vorticity equation (Mewes and Sharpio 2002) have to been neglected. This is another potentially source of error in the traditional least squares methods. Since the information associated with the time variations of the retrieval winds is ignored, the traditional least squares methods may not be accurate enough to capture the rapidly-changing wind and thermodynamic fields for a fast evolution weather process. The task of this study is to reduce the evolution-caused error in wind and thermodynamic analyses by using two successive radar volume scans.

Clearly, if the analysis space is extended to include the time dimension, then time interpolations can be easily performed and the time tendency of the wind field can be formulated in the cost function. In particular, the analyzed wind field can be expressed by a linear time interpolation between two wind fields expressed by Legendre-polynomial expansions in three spatial dimensions at the beginning time of the first volume scan and the ending time of the second volume scan. The Legendre-polynomial expansions used in this paper are the same as in MANDOP (Multiple Analytical Doppler) (Scialom and Lemaître 1990; Tabary and Scialom, 2001), but here the analysis space is extended to include the time dimension. In this extended analysis space, the wind time tendency field can be conveniently retrieved and used for the thermodynamic retrievals. As will be demonstrated in this paper, this extension can improve the time interpolation, reduce the error caused by neglecting the weather system evolution in the traditional methods, and increase the accuracy of the dynamic constraints by recovering the time tendency terms in the momentum and/or vorticity equations. The method is introduced in the next section. The merits of the method are demonstrated by numerical experiments with simulated radar observations in section 3 and the method is applied to real radar data in section 4. Conclusions follow in section 5.

2. Methodology and formulations

2.1 *Winds field retrieval*

The traditional three-dimensional variational method (3DVar) is extended to estimate two wind fields from two successive volume scans of radial-wind observations by minimizing the following cost function:

$$J = J_{\rm O} + J_{\rm CON} + J_{\rm B} + J_{\rm VE} \ , \tag{1}$$

where $J_{\rm O}, J_{\rm CON}, J_{\rm B}$ and $J_{\rm VE}$ are the observation, continuity equation, background and vertical equation constraints, correspondingly. The specific form of $J_{\rm O}$ is given by

$$J_{\rm O} = \sum_{m=1}^{M} w_{\rm O}[v_{{\rm a},r}(x_m, t_m) - v_{{\rm o},r}(x_m)]^2 \ , \tag{2}$$

where $w_{\rm O}$ is the weight of each measurement, $v_{{\rm o},r}(x_m)$ is the observed radial-wind (between two successive volume scans) at $x_m = (x_m, y_m, z_m), m = 1, 2, \ldots, M_1, M_1 + 1, M_1 + 2, \ldots M, M = M_1 + M_2$; $v_{{\rm a},r}(x_m, t_m)$ is the analyzed radial-wind at x_m. The subscript m denotes the sequence of radar measurements in four-dimensional space (x, t), the m-th measurement point is denoted by (x_m, t_m), M_1 and M_2 are the total number of measurements in the first and second volume scans, respectively. The two wind fields to be estimated are at two time levels: the beginning $t = t_1$ of the first volume scan (u_1, v_1, w_1) and the ending $t = t_M$ of the second volume scan (u_2, v_2, w_2). In this paper, each component of the two analyzed wind fields is a continuous function of $x = (x, y, z)$ in Cartesian coordinates over the analysis domain. An analytical form of each component is given by Legendre-polynomial expansions in three spatial dimensions (see Appendix). The analyzed radial-wind at $t = t_1$ is then given by

$$v_{{\rm a},r}(x_m, t_1) = d_1 u_1(x_m) + d_2 v_1(x_m) + d_3 w_1(x_m) \ , \tag{3}$$

where (d_1, d_2, d_3)=$(x/r, y/r, z/r)$ are direction cosines, $r = (x^2 + y^2 + z^2)^{1/2}$ is the radial distance from the radar. Similarly, the analyzed radial-wind field at $t = t_M$ is given by

$$v_{{\rm a},r}(x_m, t_M) = d_1 u_2(x_m) + d_2 v_2(x_m) + d_3 w_2(x_m) \ . \tag{4}$$

After the above preparations, the analyzed radial-wind at (x, t) can be obtained by the following linear time-interpolation, and then the time dimension is included into the analysis space. The analyzed radial-wind field

$v_{a,r}(x_m, t_m)$ is expressed by

$$v_{a,r}(x_m, t_m) = \alpha_1 v_{a,r}(x_m, t_1) + \alpha_2 v_{a,r}(x_m, t_M) \ , \quad (5)$$

where

$$\alpha_1 = \frac{t_M - t_m}{t_M - t_1} \ , \qquad \alpha_2 = \frac{t_1 - t_m}{t_M - t_1} \ . \quad (6)$$

The $J_{\rm CON}$ term in Eq. (1) has two parts:

$$J_{\rm CON} = \sum_{n=1}^{N} w_{\rm C_1} C_1^2 + w_{\rm C_2} C_2^2 \ , \quad (7)$$

where $w_{\rm C_1}$ and $w_{\rm C_2}$ are the weights of continuity equation constrains at two time levels t_M and t_1, respectively. N is the total number of grid points and C_1 and C_2 are continuity equations with the following correspondence:

$$C_1 = \frac{\partial u_1}{\partial x} + \frac{\partial v_1}{\partial y} + \frac{\partial w_1}{\partial z} - q w_1 \quad (8)$$

$$C_2 = \frac{\partial u_2}{\partial x} + \frac{\partial v_2}{\partial y} + \frac{\partial w_2}{\partial z} - q w_2 \ , \quad (9)$$

where $q = \partial \ln p / \partial z$, and for the standard atmosphere, q=10^{-4} m^{-1}.

The $J_{\rm B}$ term in Eq. (1) represents the constraints at the bottom and top boundaries of the analysis domain where the vertical velocity must be zero. This term is expressed as

$$J_{\rm B} = \sum_{n_f=1}^{N_f} w_{\rm B_1} w_1^2 + w_{\rm B_2} w_2^2 \ , \quad (10)$$

where N_f is the total number of grid points on the top and bottom boundary and $w_{\rm B_1}$ and $w_{\rm B_2}$ are weights of the background at t_M and t_1, respectively.

The fourth term in Eq. (1) is the constraint due to the vertical vorticity equation:

$$J_{\rm VE} = \sum_{n=1}^{N} w_{\rm VE} E^2 \ , \quad (11)$$

where $w_{\rm VE}$ is the weight of this term. According to Mewes and Shapiro (2002), the vertical-vorticity equation is given by

$$E = \frac{\partial \zeta}{\partial t} + u\frac{\partial \zeta}{\partial x} + v\frac{\partial \zeta}{\partial y} + w\frac{\partial \zeta}{\partial z} + (\zeta + f)\left(\frac{\partial u}{\partial x} + \frac{\partial u}{\partial y}\right) + \left(\frac{\partial w}{\partial x}\frac{\partial v}{\partial z} - \frac{\partial w}{\partial y}\frac{\partial u}{\partial z}\right) \ , \quad (12)$$

where ζ is the vertical vorticity. The vertical vorticity equation constraints in dual-Doppler analyses can improve retrievals of the vertical velocity and further the retrievals of perturbation pressure and temperature (Protat and Zawadzki, 2000), especially in data-void areas. Also, these constraints include the second-order derivation of wind fields so that the noise associated with raw radar data may be filtered out to some extent. However, with the traditional methods, it is difficult to estimate the local time derivative in Eq. (12) from real radar observations (Mewes and Shapiro, 2002). In this paper, since two wind fields are retrieved, the time derivative of ζ can be conveniently expressed by the two wind fields at t_M and t_1 in analysis space.

Since the analyzed winds are expressed as polynomial expansions, the control variables in the cost function are the expansion coefficients of basis functions. When the gradient formulation of the cost function is derived from Eqs. (1)–(12), the coefficients of the basis functions of the two wind fields can be obtained by minimizing the cost function (Qiu and Xu, 1996; Gao et al., 1999). The coefficients can be solved in the following steps:

(1) Choose the first guess of the coefficients (in our experiments, the first guess is set to zero).

(2) Calculate the cost function and its gradient.

(3) Use a conjugate-gradient method to update the values of the coefficients.

(4) Check if the convergence criterion is satisfied using the value of the cost function or its gradient. If not, repeat (2) and (3); if yes, the optimal coefficients are obtained.

2.2 *Thermodynamic fields retrieval*

The basic momentum equations can be written as follows:

$$c_p \theta_0 \frac{\partial \pi_*}{\partial x} = -\left(\frac{Du}{Dt} - fv - S_x\right) = A \ , \quad (13)$$

$$c_p \theta_0 \frac{\partial \pi_*}{\partial y} = -\left(\frac{Dv}{Dt} + fu - S_y\right) = B \ , \quad (14)$$

$$c_p \theta_0 \frac{\partial \pi_*}{\partial z} = -g\frac{\theta^*}{\theta_0} = -\left(\frac{Dw}{Dt} - S_z\right) = C \ , \quad (15)$$

where the variables to be estimated are the nondimensional perturbation pressure π_* and potential temperature θ_*, c_p is the specific heat at constant pressure, θ_0 the potential temperature of the reference state (given by a sounding profile), g stands for the gravity, and the three S-terms represent turbulent diffusion. Since A, B, and C are functions of the retrieved wind fields, π_* and θ_* at the middle time of two successive volume scans can be estimated from the two retrieved wind fields by using Eqs. (13)–(15).

The π_* and θ_* fields in Eq. (13)–(15) are expressed by the polynomial expansions in (A2) and then substituted into the following cost function:

$$J_{\rm PT} = J_{\rm M} + J_{\rm BPT} \ . \quad (16)$$

The first term $J_{\rm M}$ is the weak-form constraint provided by the three momentum equations, that is,

$$J_{\rm M}=\sum_{n=1}^{N}\left[w_{\rm M_1}\left(c_p\theta_0\frac{\partial\pi_*}{\partial x}-A\right)^2+w_{\rm M_2}\left(c_p\theta_0\frac{\partial\pi_*}{\partial y}-B\right)^2+w_{\rm M_3}\left(c_p\theta_0\frac{\partial\pi_*}{\partial z}-g\frac{\theta_*}{\theta_0}-C\right)^2\right], \quad (17)$$

where $w_{\rm M_1}, w_{\rm M_2}$ and $w_{\rm M_2}$ are the weights of each equation. This term alone is not sufficient to determine the two unknown fields π_* and θ_*. As shown in Gal-Chen (1978) and Brandes (1984), solving π_* and θ_* from the momentum equations can be converted to a problem of solving a 3D Poisson equation. Mathematically, solving for π_* and θ_* from the three momentum equations (13)–(15) requires π_* and θ_* or their derivatives given at the boundaries of the analysis domain. In this paper, boundary conditions of the second-kind (derivative) (Lattes and Lions, 1969) are used as weak-form constraints in the cost function to uniquely determine π_* and θ_*. The associated boundary constraint term in the cost function has the following form:

$$J_{\rm BPT}=\sum_{n_g}^{N_g}\left\{w_{\rm BP}\left[\left(\frac{\partial\pi^*}{\partial x}\right)^2+\left(\frac{\partial\pi^*}{\partial y}\right)^2+\left(\frac{\partial\pi^*}{\partial z}\right)^2\right]+w_{\rm BT}\left[\left(\frac{\partial\pi^*}{\partial x}\right)^2+\left(\frac{\partial\pi^*}{\partial y}\right)^2+\left(\frac{\partial\pi^*}{\partial z}\right)^2\right]\right\}, \quad (18)$$

where N_g is the total number of grid points on the boundary and $w_{\rm BP}$ and $w_{\rm BT}$ are the weights for perturbation pressure and temperature, respectively. This weak-form boundary constraint is different from the weak-form used by Brandes (1984), so the retrieved fields will not be overly suppressed along the boundaries. Similar to the wind retrieval, the control variables are coefficients of a basis function, which can be solved by using the same optimization procedures.

In the traditional wind and thermodynamic retrieval methods (TWTM), the wind field is retrieved at a single time level. The thermodynamic fields are then derived from the retrieved wind field at the same single time level. Thus, the time tendency terms in the momentum equation are ignored. As pointed out by Liou (2001), errors of the TWTM thermodynamic retrievals caused by neglecting the time tendency terms can be very large, especially when the radar scan period is larger than 5 min. By including the time dimension in the analysis space, the method developed in this paper recovers the time tendency terms in the momentum and vorticity equations. This method will be called the extended 3DVar wind and thermodynamic method (EWTM). The merits of EWTM are shown by numerical experiments with simulated radar data in the next section.

3. Experiments with simulated radar data

3.1 *Simulated radar data*

The Advanced Regional Prediction System (ARPS; Xue et al., 1995) is employed to generate simulated radar data for an extensively studied supercell storm that occurred on 20 May 1977 in the Del City storm in Oklahoma. A detailed description of the storm development can be found in Mewes and Shapiro (2002). The model domain size is $64\times64\times15$ km^3. The grid interval is 1.0 km in the horizontal and 0.5 km in the vertical. The storm is initiated by a thermal bubble from the sounding, centered at x=48 km, y=16 km and z=1.5 km where the coordinate origin is at the lower front left corner of the grid.

The simulation shows that the thermal bubble grows into a loosely-organized convective cell at t=1200 s and then evolves gradually into a well-organized multi-cell system. Simulated radar data are generated from t=6600 to 7200 s. The analysis domain covers only the primary supercell storm, which is limited to $20\times20\times15$ km^3 within the model domain. A vertical cross section of the simulated wind field is shown in Fig. 1a at t=6600 s and x=10 km, while the perturbation pressure and temperature are shown in Fig. 1b and 1c at t=6900 s and x=10 km, where the coordinate origin is at the front lower left corner of the analysis domain. As shown, the main updraft is quite strong but the downdraft near the right lower corner is weak and fully developed at this time, indicating that the supercell is nearly mature.

The two radars are located at (10, 40, 0.0) and (40, 10, 0.0) km, respectively, where the coordinate origin is at the front lower left corner of the analysis domain at the initial time for each analysis period. To mimic the Next Generation Radar (NEXRAD) severe storm radar-scanning mode, each simulated radar volume scan consists of 14 elevations from 0.5° to 20° with an azimuthal resolution of 1° and range gate interval of 250 m. Each volume scan is completed in 5 minutes with each beam position determined and timed accurately for the simulated radar observations.

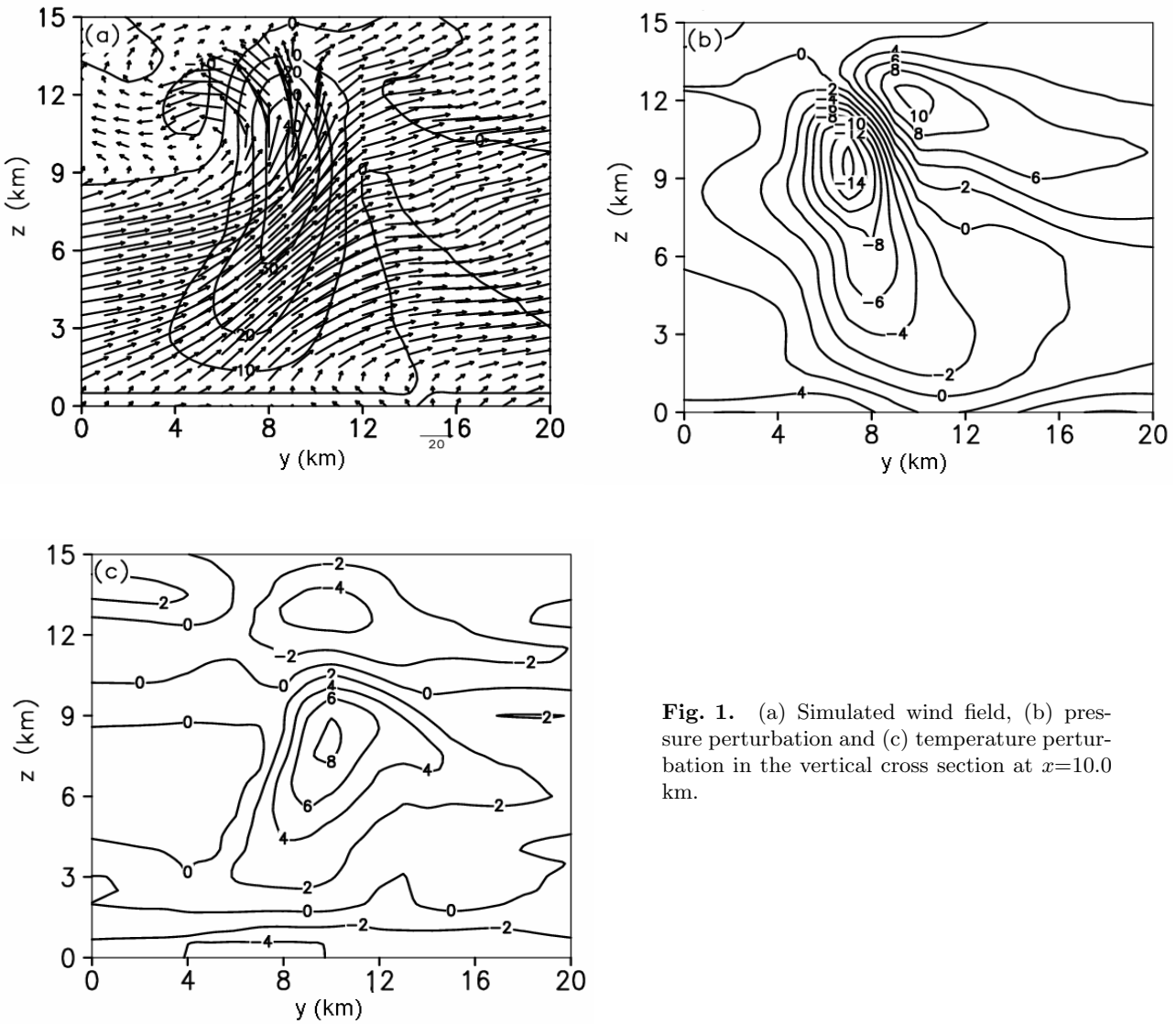

Fig. 1. (a) Simulated wind field, (b) pressure perturbation and (c) temperature perturbation in the vertical cross section at x=10.0 km.

3.2 *Retrieved wind and thermodynamic fields*

By using the above simulated radar data, wind analyses are performed by EWTM and TWTM. The truncation number of the Legendre expansion is set to seven in each direction. The remaining parameter settings for the two methods are given as follows: $w_{\mathrm{O}} = 1.0, w_{\mathrm{C}_1} = w_{\mathrm{C}_2} = 1.0 \times 10^5, w_{\mathrm{B}_1} = 10.0, w_{\mathrm{B}_2} = 1.0, w_{\mathrm{VE}} = 10.0, w_{\mathrm{M}_1} = w_{\mathrm{M}_2} = 1.0, w_{\mathrm{M}_3} = 0.5$ and $w_{\mathrm{BP}} = w_{\mathrm{BT}} = 10.0$. These values depend on the error statistics of their associated terms. A large number of numerical experiments are carried out to test the sensitivity of analysis error to each parameter. The results indicate that the analysis error is not very sensitive to the boundary constraints parameters $(w_{\mathrm{B}_1}, w_{\mathrm{B}_2}, w_{\mathrm{BP}}, w_{\mathrm{BT}})$. Also, when the orders of magnitude of the continuity equation and vorticity equation constraints are comparable with that of the observation term, a good result can be obtained.

The performances of the two methods can be evaluated by correlation coefficient [CC, as defined in Eq. (4) of Xu et al., 2001] of the analyzed three-dimensional wind and thermodynamic fields with respect to the model simulated. Their values are listed in Table 1. The horizontal wind u and v are well retrieved by the two methods and their CCs are larger than 90%. The CCs of the horizontal winds (u and v) obtained by EWTM are slightly better than those by TWTM. However, there is considerable difference in the vertical wind and thermodynamic fields from the two methods. As shown, the CCs of the vertical velocity at t = 6600 s and t = 7200 s are about 5% larger than those obtained by TWTM. Also, the CCs of the perturbation pressure and temperature obtained by EWTM are about 4% and 8% higher than those by

Table 1. The correlation coefficients between the retrieved and simulated fields.

Method	t=6600 s		t=7200 s		t=6900 s	
	u and v	w	u and v	w	π_*	θ_*
TWTM	0.932	0.695	0.924	0.663	0.822	0.502
EWTM	0.958	0.741	0.950	0.719	0.860	0.589

Table 2. The same as Table 1 but for 7.5 min radar volume scan period.

Method	t=6450 s		t=7350 s		t=6900 s	
	u and v	w	u and v	w	π_*	θ_*
TWTM	0.922	0.650	0.914	0.621	0.812	0.486
EWTM	0.938	0.731	0.942	0.703	0.840	0.568

Table 3. The same as Table 1 but for 2.5 min rader volume scan period.

Method	t=6750 s		t=7050 s		t=6900 s	
	u and v	w	u and v	w	π_*	θ_*
TWTM	0.952	0.726	0.944	0.695	0.832	0.572
EWTM	0.964	0.758	0.956	0.726	0.860	0.609

TWTM, respectively. During the analysis period, the storm intensified rapidly especially in its vertical velocity. This may cause a relatively large error in the TWTM retrieved vertical velocity due to its single-time treatment and related approximations. In addition, since the perturbation temperature is constrained mainly by the vertical momentum equation (15), the analyzed vertical velocity will directly affect the temperature retrieval. This explains why the EWTM gives largest improvement in the perturbation temperature field among all the retrieved component fields. The EWTM-analyzed vertical wind and thermodynamic fields are shown in Fig. 2 in comparison with the TWTM-analyzed ones in Fig. 3. The EWTM-analyzed fields show a strong updraft with positive temperature perturbation (Fig. 2c) within the updraft (Fig. 2a) at the middle level. The pressure perturbation (Fig. 2b) is negative (positive) in the rear (front) side of the storm. The retrieved fields capture almost all characteristics of the simulated storm. The updraft and positive temperature perturbation in Fig. 3a are clearly weaker than those in Fig. 2a. The differences of vertical velocity and perturbation temperature at $x = 10$ km between simulated and EWTM-analyzed fields are shown in Fig. 4a and Fig. 4c and those between simulated and TWTM-analyzed fields are shown in Fig. 4b and Fig. 4d. The structures of the difference fields from the two methods are similar. The maximum speeds of the difference fields in Fig. 4a and 4b are near the updraft core and are 15 m s^{-1} and 25 m s^{-1} for EWTM and TWTM, respectively. Near the same region, the difference of perturbation temperatures from the EWTM method is 2° smaller than that from the TWTM method. Since the supercell evolves fast near the updraft core, the EWTM method is more accurate than the TWTM method in this region. This explains why the EWTM method shows the smaller difference against the simulated field than the TWTM method.

Clearly, the performance of the EWTM method depends on the radar volume scan period. To examine the sensitivity of the EWTM method to volume scan period, 2.5 min and 7.5 min volume scan period radar data are generated, respectively. The first set of data are from t=6750 s to 7050 s and the second set are from t=6450 s to 7350 s. The thermodynamic fields to be retrieved are at the same time as the above experiment. The results of the two methods are listed in Table 2 and Table 3, respectively. As shown, when the volume scan period becomes short (2.5 min), the difference between EWTM and TWTM decreases; when the volume scan period becomes large (7.5 min), the difference between the two methods increases. However, we have to point out that the performance of the EWTM method should depend rely on the timescale of the observed weather system too. The timescale of the simulated supercell is near 60 min and is significantly larger than the volume scan period used in our experiments. Thus, the linear evolution assumption in the wind field is valid and EWTM is better than TWTM. If the timescale of the concerned weather system is comparable with the radar volume scan period, the

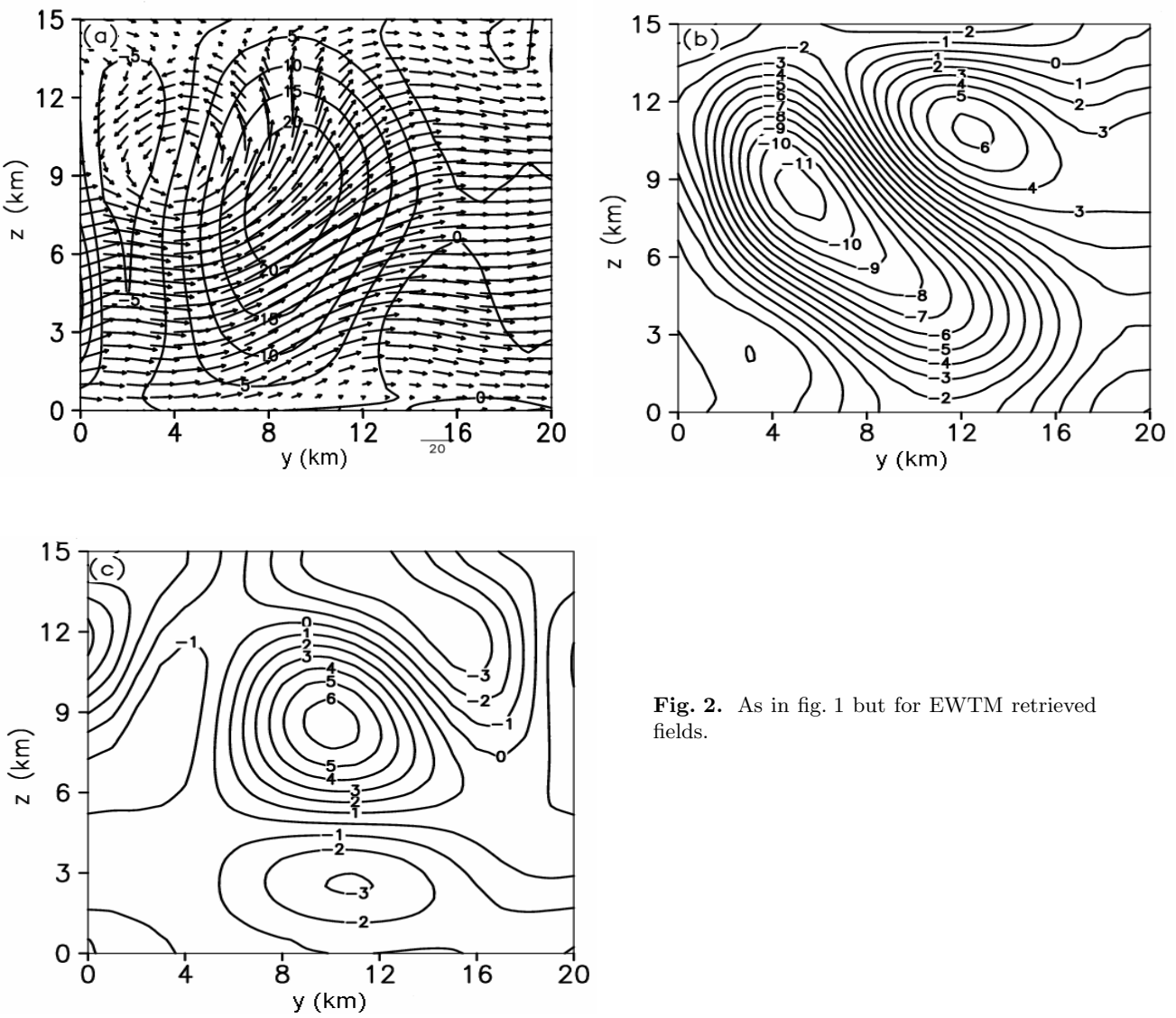

Fig. 2. As in fig. 1 but for EWTM retrieved fields.

linear evolution assumption may not be accurate and the merit of EWTM will disappear. However, for most weather systems, their timescale are larger than the 5–10 min volume scan period used in current operational radar networks, so the ETWM method can be applied.

In this section, numerical experiments are performed with simulated radar data. The results demonstrate that the EWTM can improve the accuracy of the wind and thermodynamic retreivals in comparison with the traditional method. In the next section, the EWTM method is further tested with real Doppler velocity data.

4. Real-case experiment

Radar observations of a Meiyu front heavy rainfall during the China Heavy Rain Experiment (CHeRES) are used to test the new (EWTM) method. This heavy rainfall event occurred on 22 June 2002 and the storm winds were observed by two Doppler radars. The two radars are located at Yichang (30.70°N, 111.29°E) and Jinzhou (30.70°N, 111.29°E) in China, respectively. The former is an S-band radar and the latter is a C-band radar. During this event, the rainstorm formed and produced heavy rainfall in the Changjiang–Huaihe basin in the East of China. The radar raw data are preprocessed with quality control and velocity dealiasing (James and Houze, 2001). Two volume scans from each radar are used in the analysis. The beginning time and the ending time of the two volume scans from the Yichang radar are 1118 (LST) and 1130 (LST); those from Jinzhou radar are 1119 (LST) and 1130

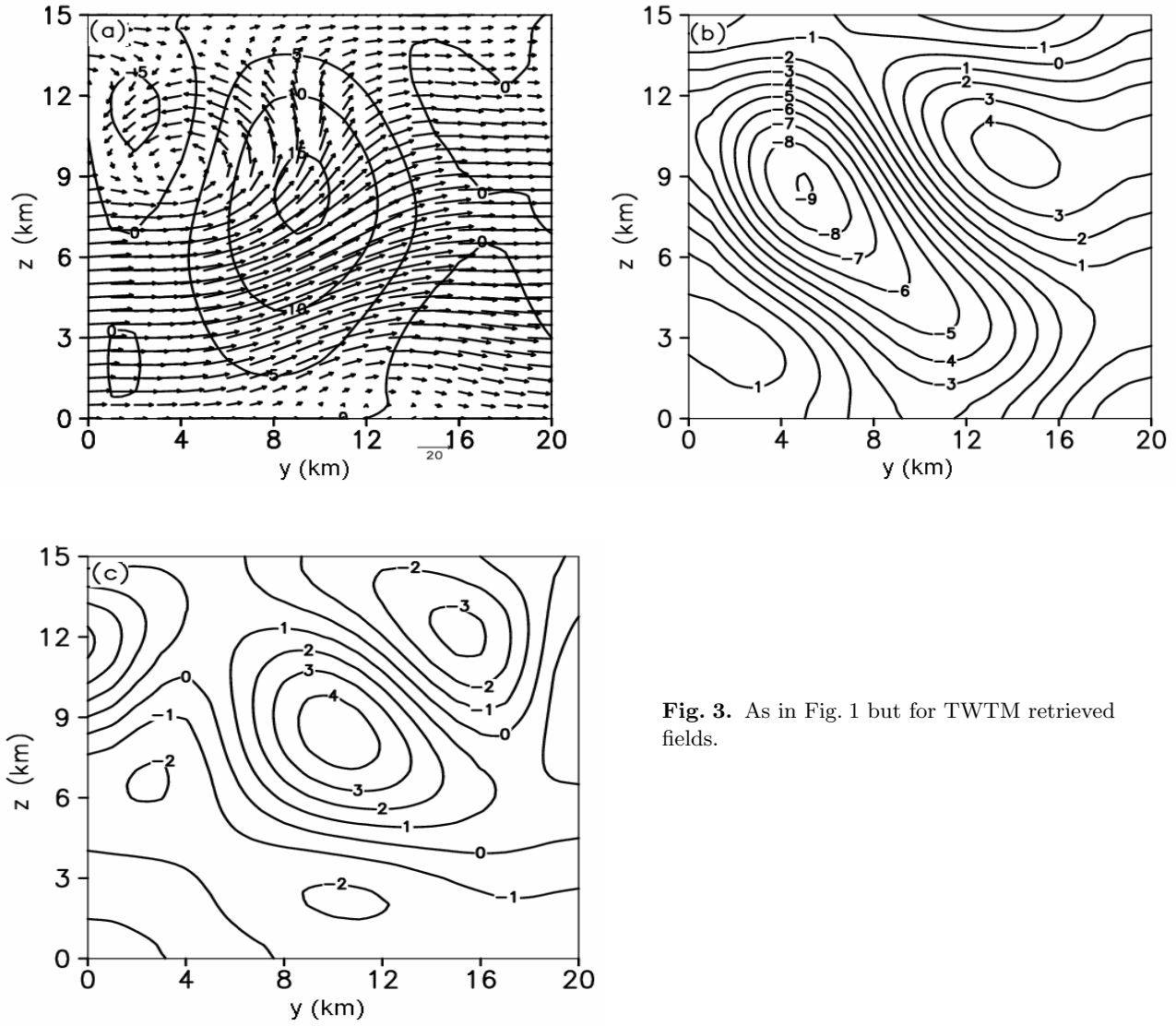

Fig. 3. As in Fig. 1 but for TWTM retrieved fields.

(LST). The analysis domain is $80\times80\times9.5$ km^3. The origin (0, 0, 0) is set at the lower left corner of the analysis domain, in which the Yichang radar is located at (–13.0, 1.0, 0.0) and the Jinzhou radar is at (18.80, –25.60, 0.0).

The horizontal cross section (at $z = 1.5$ km) of reflectivity at 1124 (LST) from the Yichang radar is shown in Fig. 5a, in which the maximum reflectivity is above 35 dBZ in the heavy rainfall region which is located at $30 < x < 50$ km and $20 < y < 50$ km. Figure 5b shows the retrieved wind field (vectors) and the observed radial velocity (contours) from the Yichang radar. As shown, a wind shift-line takes a northeast-southwest direction. One side of the wind shift-line is a southerly wind and the other side a north-northeastern wind. The maximum/minimum value of the retrieved v component is about 12/–2 m s^{-1} on the north/south side of the wind shift-line, so the wind shift is very strong. This wind shift-line follows closely the zero contour of the observed radial velocity (Fig. 5b). Note that the zero contour of the observed radial velocity is to the southeast of the radar (outside the analysis domain), so the strong gradient of the observed radial velocity in the vicinity of the zero contour line implies the existence of strong local convergence. This feature and implied convergence are well captured and quantified by the retrieved vector wind field. The wind shift-line in the retrieved wind field (Fig. 5b) is also consistent with the boundary of the heavy rainfall region as indicated by the observed reflectivity in Fig. 5b.

The retrieved perturbation pressure and tempera-

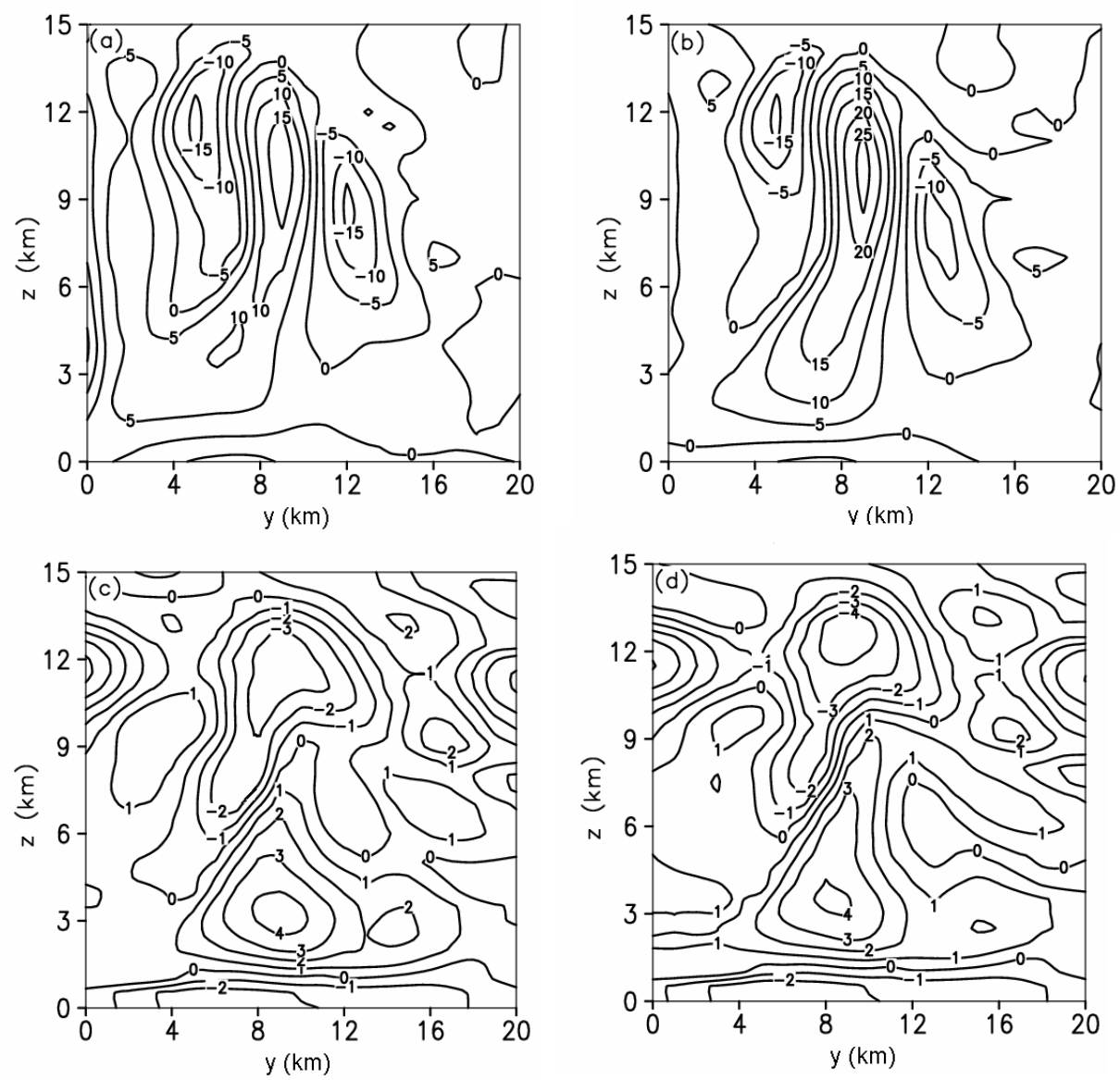

Fig. 4. The differences of vertical velocity (a) between simulated and EWTM-analyzed fields and (b) between simulated and TWTM-analyzed fields; (c) and (d) similar to (a) and (b) but for the differences of perturbation temperature.

ture are shown in Fig. 5c and Fig. 5d, respectively. As shown in Fig. 5c, the perturbation pressure increases from northwest to southeast over the analysis domain. This pressure gradient agrees with the large-scale environment dominated by a strong western Pacific subtropical high located to the east of the analysis domain. This pressure gradient is also consistent with the overall southwesterly wind over the analysis domain. As shown in Fig. 5d, the retrieved perturbation temperature field is characterized mainly by a negative center in the rainfall region. This negative center could be explained by the evaporative cooling in the lower-level precipitation-induced downdraft region.

Figure 6 shows the vertical cross sections (at $x = 40$ km) of the retrieved wind and thermodynamic fields. The retrieved (v, w) vector winds (with w amplified 10 times for display) and w contours (Fig. 6a) show that there is a slantwise frontal boundary between the ascending and descending flows. The front is slanted northward. The maximum vertical velocity of the ascending flow is 1.2 m s^{-1}. The maximum negative vertical velocity of the descending flow is –0.5 m s^{-1}. As shown in Fig. 6b, the retrieved perturbation pressure is negative along the main ascending flow immediately

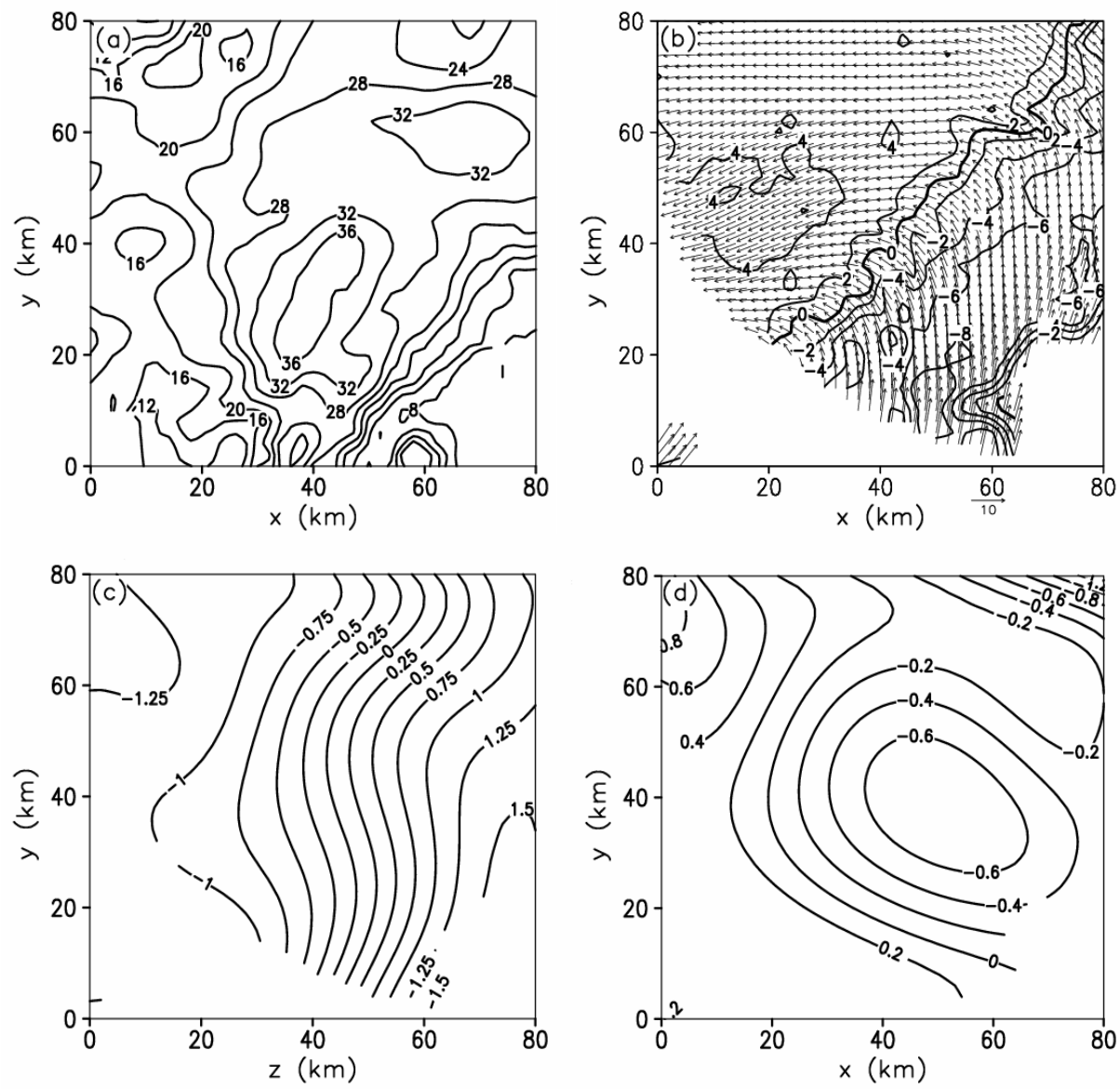

Fig. 5. (a) The horizontal cross section of reflectivity from the Yichang radar, (b) EWTM-retrieved wind and radial-wind contours, (c) EWTM-retrieved pressure perturbation, and (d) temperature perturbation at $z = 1.5$ km.

above the frontal boundary but becomes positive further high-up away from the frontal boundary in the ascending region. The negative perturbation pressure could be a mesoscale feature related to the local buoyancy production due to the latent heating in the main ascending flow immediately above the frontal boundary. The positive perturbation pressure aloft may be related to the large-scale environment dominated by a strong western Pacific subtropical high. Below the frontal boundary, the retrieved perturbation pressure is positive near the ground in the precipitation-induced downdraft region. This positive perturbation pressure could be related to the cold pool in the downdraft region (Fig. 6c). The retrieved perturbation temperature is positive in the ascending flow and negative in the descending flow. These general features in the retrieved fields are consistent with the conceptual model of a Meiyu front, but some detailed mesoscale aspects in the retrieved fields are not verified due to lack of other independent observations.

5. Conclusions

A variational method is developed for wind and

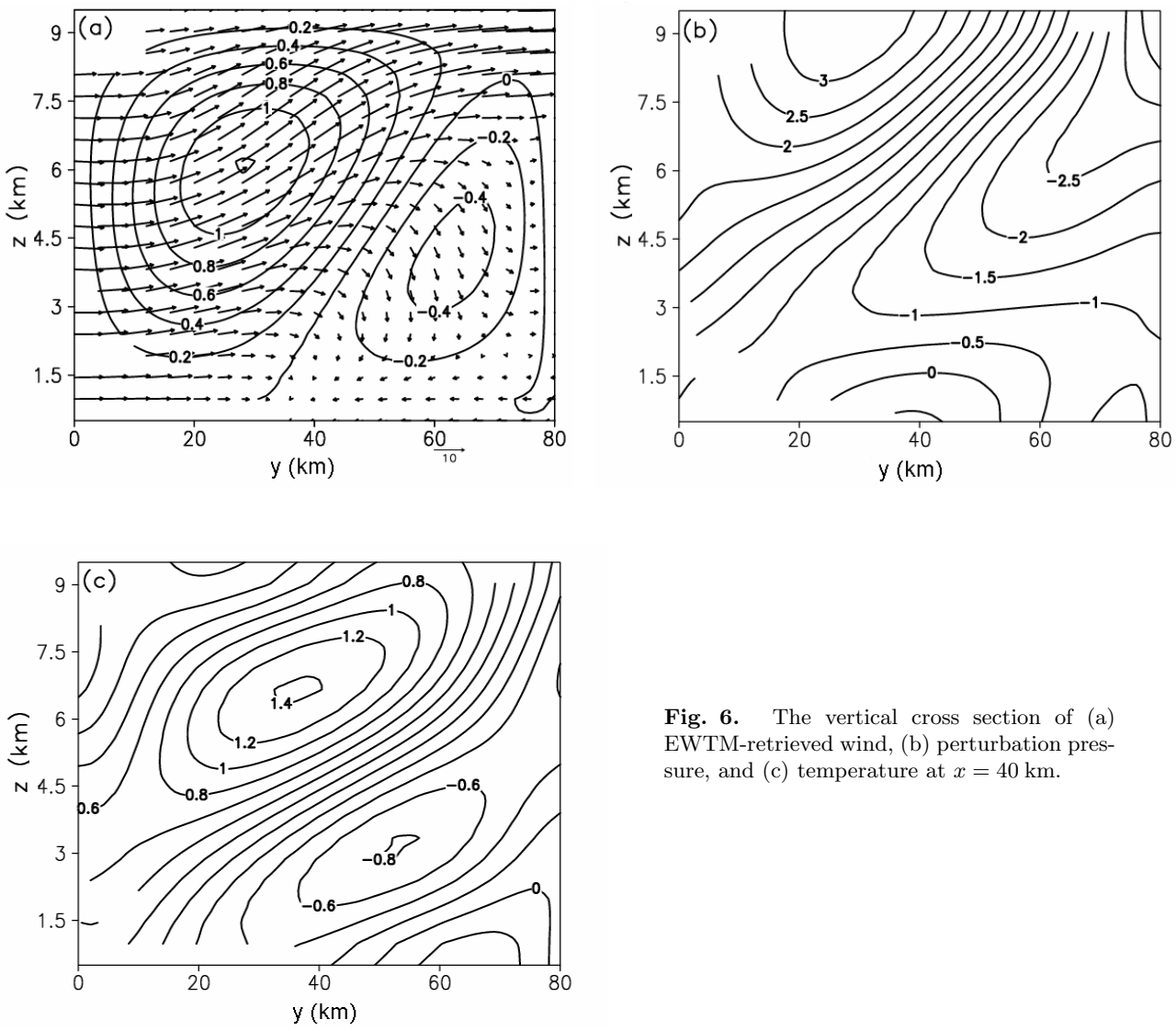

Fig. 6. The vertical cross section of (a) EWTM-retrieved wind, (b) perturbation pressure, and (c) temperature at $x = 40$ km.

thermodynamic retrievals from Doppler radar observations. This method contains two steps. The first step retrieves, from two successive volume scans, two wind fields simultaneously at the beginning and ending times of the retrieval time window by using the weak form constraints provided by the mass continuity and vorticity equations. The second step derives thermodynamic fields from the retrieved wind fields. In comparison with the traditional least squares method, the analysis space in this new method is extended from three spatial dimensions to four space-time dimensions for the wind retrievals. This extension improves the time interpolation and reduces the error caused by the traditional methods that neglect the time evolution of the observed weather system. This extension also allows the recovery of the time tendency terms in the momentum and/or vorticity equations and thus increases the accuracy of the dynamic constraints. In addition, since the retrieved wind and thermodynamic fields are expressed by truncated expansions of Legendre basis functions, short-wave noise is filtered without using other smoothing constraints in the cost function. The truncated expansions also reduce the number of unknowns effectively and thus improve the reliability of the retrievals.

The new method is tested first with simulated radar observations. The test results show that the new method is able to capture the rapid variations of the wind fields during the retrieval time window (covering two successive volume scans) and improve the accuracy of the wind and thermodynamic retrievals, especially in the vertical velocity and temperature re-

trievals, in comparison with the traditional method. The method is then applied to real radar data collected for a heavy rainfall event during the 2001 meiyu season in China. The retrieved wind and thermodynamic fields reveal the slantwise structures of the meiyu front and its associated warm ascending flow (ahead and above the slanted front) and cold descending flow (behind and below the slanted front). While these general features in the retrieved fields are consistent with the conceptual model of a meiyu front, some detailed mesoscale aspects in the retrieved fields are not verified due to lack of other independent observations. This calls for further studies and verifications beyond the current study.

Acknowledgments. This research was supported by the FAA contract IA# DTFA03-01-X-9007 to the National Sever Strorms Laboratory (NSSL), by the National Science Foundation (NSF) Grant ATM-9983077 and by the National Natural Science Foundation of China Grant No.40175010.

APPENDIX

Three-dimensional Legendre-polynomial expansions

$f(x)$ is a continuous function in three-dimensional space, which can be expressed by a three-dimensional expansion of Legendre-polynomials in Cartesian coordinates over the analysis domain as follows:

$$f(x);\ \sum_{k=1}^{T_z}\sum_{j=1}^{T_y}\sum_{i=1}^{T_x} c_{i,j,k}p_i(x)p_i(x)p_j(y)p_k(z)\ , \quad \text{(A1)}$$

where $p_i(x), p_j(y), p_k(z)$ denote the i-th, j-th, k-th Legendre-polynomial, respectively $c_{i,j,k}$ is the expansion coefficients, and T_x, T_y, T_z the truncation number in each direction. Rearrange (A1) to get:

$$f(x);\ \sum_{t=1}^{T} c_t g_t(x)\ , \quad \text{(A2)}$$

where $T = T_x + T_y + T_z$, $c_t = c_{i,j,k}$ and $g_t = p_i(x)p_j(x)p_k(x)$.

REFERENCES

Brandes, Edward A., 1984: Relationships Between Radar-Derived Thermodynamic Variables and Tornadogenesis. *Mon. Wea. Rev.*, **112**, 1033–1052.

Clark, T. L., F. I. Harris, and C. G. Mohr, 1980: Errors in wind fields derived from multiple-Doppler radars: Random errors and temporal errors associated with advection and evolution. *J. Appl. Meteor.*, **19**, 1273–1284.

Gal-Chen, T., 1978: A method for the initialization of the anelastic equations: Implications for matching models with Observations. *Mon. Wea. Rev.*, **106**, 587–606.

Gao, J., M. Xue, A. Shapiro, and K. K. Droegemeier, 1999: A variational method for the analysis of three-dimensional wind fields from two Doppler radars. *Mon. Wea. Rev.,* **127**, 2128–2142.

James, C., and R. Houze, 2001: A Real-Time Four-Dimensional Doppler Dealiasing Scheme. *J. Atmos. Oceanic Technol.*, **18**, 1674–1683.

Laroche, S., and I. Zawadzki, 1994: A variational analysis method for retrieval of three-dimensional wind field from single-Doppler radar data. *J. Atmos. Sci.,* **51**, 2664–2682.

Lattes, R., and J. Lions, 1969: *The Method of Quasi-Reversibility, Applications to Paritial Differential Equations*. American Elsevier, New York, 388pp.

Liou, Y., 1999: Single radar recovery of cross-beam wind components using a modified moving frame of reference technique. *J. Atmos. Oceanic Technol.*, **16**, 1003–1016.

Liou, Yu-Chieng, 2001: The Derivation of absolute potential temperature perturbations and pressure gradients from wind measurements in three-dimensional space. *J. Atmos. Oceanic Technol.*, **18**, 577–590.

Liou, Y., C. Tai-Chi, and K. Chung, 2003: A three-dimensional variational Approach for deriving the thermodynamic structure using Doppler wind observations—An application to a subtropical squall line. *J. Appl. Meteor.*, **42**, 1443–1454.

Mewes, T., and Shapiro., 2002: Use of the vorticity equation in dual-Doppler analysis of the vertical velocity field. *J. Atmos. Oceanic Technol.*, **19**, 543–567.

Protat, A., and I. Zawadzki, 1999: A variational method for real-time retrieval of three-dimensional wind field from multiple-Doppler bistatic radar network data. *J. Atmos. Oceanic Technol.,* **16**, 432–449.

Protat, A., and I. Zawadzki, 2000: Optimization of dynamic retrievals from a multiple-Doppler radar network. *J. Atmos. Oceanic Technol.,* **17**, 753–760.

Qiu Chongjian., and Q. Xu, 1996: Least-square retrieval of microburst winds from single-Doppler radar data. *Mon. Wea. Rev.*, **124**, 1132–1144.

Scialom, G., and Y. Lemaître, 1990: A new analysis for the retrieval of three-dimensional mesoscale wind fields from multiple Doppler radar. *J. Atmos. Oceanic Technol.,* **7**, 640–665.

Shapiro, A., S. Ellis, and J. Shaw, 1995: Single-Doppler velocity retrievals with Phoenix II data: Clear air and microburst wind retrievals in the planetary boundary layer. *J. Atmos. Sci.*, **52**, 1265–1287.

Sun, J., and N. A. Crook, 1994: Wind and thermodynamic retrieval from single-Doppler measurements of a gust front observed during Phoenix II. *Mon. Wea. Rev.*, **122**, 1075–1091.

Sun, J., and N. A. Crook, 1996: Comparison of thermodynamic retrieval by the adjoint method with the traditional retrieval method. *Mon. Wea. Rev.,* **124**, 308–324.

Tabary, P., and G. Scialom, 2001: MANDOP analysis over complex orography in the context of the MAP experiment. *J. Atmos. Oceanic Technol.*, **18**, 1293–1314.

Weygandt, S. S., A. Shapiro, and K. K. Droegemeier, 2002: Retrieval of model initial fields from single-Doppler observations of a supercell thunderstorm. Part II: Thermodynamic retrieval and numerical prediction. *Mon. Wea. Rev.*, **130**, 454–476.

Xu, Q., Qiu Chongjian, and J. Yu, 1994: Adjoint-method retrievals of low-altitude wind fields from single-Doppler reflectivity measured during Phoenix II. *J. Atmos. Oceanic Technol.*, **11**, 275–288.

Xu, Q., H. Gu, and Qiu Chongjian, 2001: Simple adjoint retrievals of wet-microburst winds and gust-front winds from single-Doppler radar data. *J. Appl. Meteor.*, **40**, 1485–1499.

Xue, M., K. K. Droegemeier, V. Wong, A. Shaprio and K. Brewster, 1995: Advanced Regional Prediction System(APPS) version 4.0 user's guide. [Available from Center for Analysis and Prediction of Storms, University of Oklahoma, 100E. Boyd, Norman, OK 73019].

Zhang, J., T. Gal-Chen, 1996: Single-Doppler wind retrieval in the moving frame of reference *J. Atmos. Sci.*, **53**, 2609–2623.